


# Direct observation of hydrogen at defects in multicrystalline silicon

David Tweddle<sup>1</sup>  | Phillip Hamer<sup>1,2</sup>  | Zhao Shen<sup>1</sup> | Vladimir P. Markevich<sup>3</sup> | Michael P. Moody<sup>1</sup> | Peter R. Wilshaw<sup>1</sup>

<sup>1</sup>Department of Materials, University of Oxford, Parks Road, Oxford OX1 3PH, UK

<sup>2</sup>School of Photovoltaics and Renewable Energy Engineering, University of New South Wales, Sydney, NSW 2052, Australia

<sup>3</sup>School of Electrical and Electronic Engineering, University of Manchester, Manchester M13 9PL, UK

## Correspondence

Hamer, P., School of Photovoltaic and Renewable Energy Engineering, University of New South Wales, Sydney, NSW 2052, Australia.  
Email: phillhamer@gmail.com

## Funding information

EPSRC, Grant/Award Number: EP/M024911/1

## Abstract

Hydrogen passivation is a key industrial technique used to reduce the recombination activity of defects in multicrystalline silicon (mc-Si). However, not all dislocations and grain boundaries respond well to traditional hydrogen passivation techniques. In order to understand the reasons for these different behaviours, and how superior passivation might be achieved, a method is required for the direct observation of hydrogen at these defects. Here, we present a novel characterisation technique based on a combination of transmission Kikuchi diffraction (TKD), atom probe tomography (APT), and isotopic substitution that enables unambiguous detection and quantification of hydrogen atoms present at crystallographic defects in mc-Si.

## KEYWORDS

atom probe tomography, crystallographic defects, defect passivation, hydrogen, silicon

## 1 | INTRODUCTION

Currently, over 60% of silicon solar cells are manufactured using multicrystalline silicon (mc-Si).<sup>1</sup> The performance of these cells is limited by carrier recombination at crystallographic defects, such as grain boundaries and dislocations, and the impurities that decorate them.<sup>2</sup> The reduction of these sources of recombination has been identified as one of the key challenges for the future of solar cell development.<sup>3,4</sup> The introduction of atomic hydrogen from dielectric layers during high temperature steps in the processing of silicon has been shown to result in increases in bulk carrier lifetime by almost an order of magnitude,<sup>5</sup> and the complete electrical deactivation of certain grain boundaries.<sup>6–9</sup>

Although hydrogen passivation is the most effective current commercial process in reducing this recombination, there remain a number of significant unanswered questions about the process.<sup>8,10</sup> In particular, it is not understood why hydrogen passivation is effective on some defects but not others.<sup>3</sup> For example, Bertoni et al,<sup>8</sup> recently showed

that while a random-angle grain boundary clearly responds to hydrogen passivation, a  $\Sigma 27$  boundary subject to the same process remains electrically active. Also, unresolved are the mechanisms by which charge carrier injection (by light or biased junctions), hydrogen and defect charge states, and/or prior gettering steps act to change the effectiveness of hydrogen passivation.<sup>11–13</sup>

The primary reason so little is known about the hydrogen passivation process is that the bulk hydrogen concentrations ( $10^{14}$ – $10^{16}$  cm<sup>-3</sup>) involved in these processes are well below the detection limits of most available techniques.<sup>14–16</sup> Indeed, the characterisation of hydrogen in material microstructure remains a formidable challenge even for modern high-resolution microscopes. This inability to directly image hydrogen, particularly at the atomic scale, has limited the understanding of its role in affecting the performance of a wide range of materials.

APT is a 3D nanoscale microscopy technique that provides both chemical identity and precise spatial location of individual atoms within a material microstructure. More specifically, recent studies have

This is an open access article under the terms of the Creative Commons Attribution License, which permits use, distribution and reproduction in any medium, provided the original work is properly cited.

© 2019 The Authors. Progress in Photovoltaics: Research and Applications published by John Wiley & Sons Ltd

demonstrated the unique insights provided by APT in the characterisation of grain boundaries within mc-Si, using a multimicroscopical approach of electron backscatter diffraction (EBSD), electron beam-induced current (EBIC), and APT.<sup>17–19</sup> Utilising these methods, recombination active random-angled grain boundaries enriched in C, O, and Cu have been observed.<sup>20,21</sup> Since APT provides both spatial and compositional information at the atomic scale, it has obvious potential to bring new insights to the mechanisms behind the hydrogen passivation of defects in silicon. However, a major drawback in the design of current atom probes is the significant amount of ambient hydrogen that is present in the analysis chamber during operation. This hydrogen adsorbs onto the specimen and is then evaporated from its surface just like the constituent atoms.<sup>22</sup> Hence, it is not possible to distinguish hydrogen present in the analysis chamber from hydrogen introduced during passivation. However, this issue can be mitigated by passivating with  $^2\text{H}$  (deuterium), which has a low natural abundance of 0.015% and can therefore be distinguished from the environmental hydrogen, which is overwhelmingly  $^1\text{H}$ .

Although APT has not previously been used to detect  $^2\text{H}$  in passivated mc-Si, a number of authors have used this approach with other materials. Takahashi et al<sup>23</sup> and Chen et al<sup>24</sup> directly observed the

presence of hydrogen trapped at nanoscale carbides in steels, while the first APT observation of  $^2\text{H}$  segregation to the grain boundary was presented by Sundell et al<sup>22</sup> in a zirconium alloy. However, in that study,  $^2\text{H}$  was detected at 18 Da in the mass-to-charge-state spectrum in the form of  $^2\text{H}^{16}\text{O}^+$  ions. This peak overlaps with  $^1\text{H}_2^{16}\text{O}^+$ , a molecule also routinely detected in APT experiments. Therefore, despite persuasive evidence provided by the authors, it was not possible to definitively confirm the presence of  $^2\text{H}$  at this oxide grain boundary.

In this study by combining hydrogen passivation, underpinned by isotopic substitution from an atomic source, with the 3D atomic-scale characterisation technique atom probe tomography (APT) and crystallographic information by transmission Kikuchi diffraction (TKD), we present a novel experimental protocol for the direct and unambiguous imaging of individual hydrogen atoms at defects within mc-Si.

## 2 | METHODS

The material used in this study is a  $2 \times 2$  cm wafer section taken from a p-type high-performance multicrystalline silicon (HPMC) ingot.<sup>2,25</sup> The surface saw damage was removed using a chemical etch of

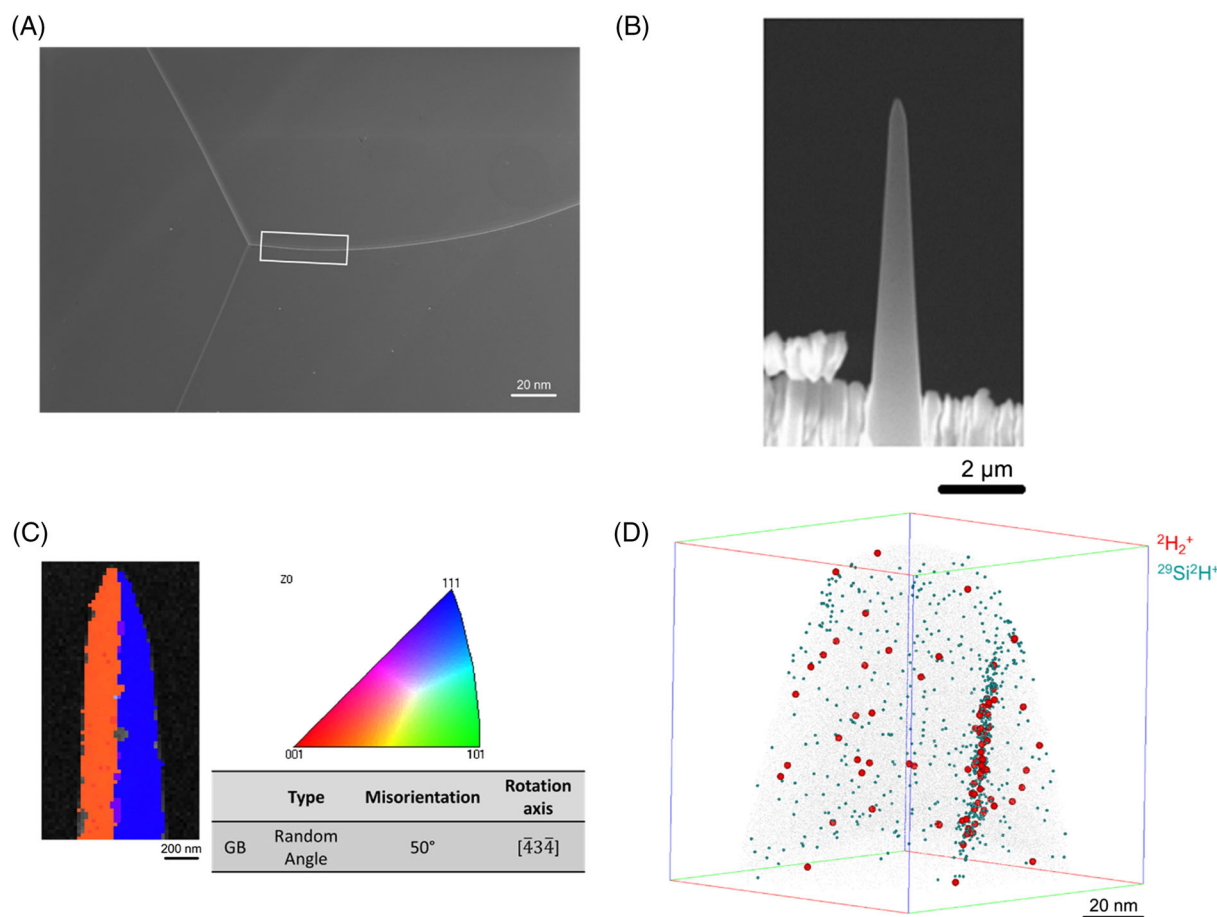


**FIGURE 1** A, Scanning electron micrograph of the Secco etched silicon sample, with the random-angle grain boundary selected for analysis marked. B, Scanning electron micrograph of the grain boundary atom probe needle. C, Inverse pole figure (IPF-Z) of the specimen, subsequent to atom probe tomography (APT) analysis with a table displaying the grain's misorientation and rotation axis. D, APT dataset showing the enrichment of  $^2\text{H}_2^+$  and  $^{29}\text{Si}^2\text{H}^+$  at a grain boundary, with a small fraction of Si atoms (grey) shown for reference

hydrofluoric acid (50 mL), nitric acid (220 mL), and acetic acid (30 mL). The samples were then etched using a Secco etch, as described in Secco d' Aragona<sup>26</sup> for 40 seconds in order to create etch pits at dislocations and grain boundaries visible under an electron microscope. The samples were then exposed to a remote  $^2\text{H}$  plasma at 200°C for 60 minutes with a plasma power of 30 W. The use of atomic  $^2\text{H}$  is important as it is much more effective at introducing hydrogen into silicon than molecular sources and more closely mimics hydrogen sources used in solar cell production.<sup>3,27,28</sup>

Atom probe samples were produced by selecting individual defects using focussed ion beam (FIB) methods via a Zeiss NVision Dual Beam SEM/FIB, after the method described in Lotharukpong et al.<sup>29</sup> This method used FIB techniques to create a lift-out bar containing the grain boundary of interest, which was then attached to the end of a transmission electron microscopy (TEM) half grid. Doughnut milling was then used for the production of needles with the grain boundary running along the length of the needle, enabling a comparatively large

section of the boundary to be analysed. TKD<sup>30–32</sup> was performed on the needles using a Zeiss Crossbeam with a beam of 30 kV and 2 nA. APT was performed using a Cameca LEAP 5000 XR with 52% detection efficiency, at a temperature of 50 K, pulse frequency of 200 kHz, laser energy of 50 pJ, and detection rate of 1.5%. APT reconstructions were calibrated using the voltage curve to estimate the radius and shank angle of the specimen, using IVAS 3.8.2. Voltage pulsing mode has previously been utilised in the APT analysis of metal alloys to reduce the effects of mass spectrum overlaps caused by complex ions and thereby simplify the quantification of  $^2\text{H}$ . However, this must be balanced with specimen viability, which is of increasing consequence when combining APT with correlative analyses on the same tip. The silicon materials analysed in this work have been found to be significantly less viable to APT analysis under such experimental conditions, and hence, laser pulsing was implemented instead. Furthermore, it is shown in this study that the use of laser pulsing to examine these silicon samples did not prevent isolation of

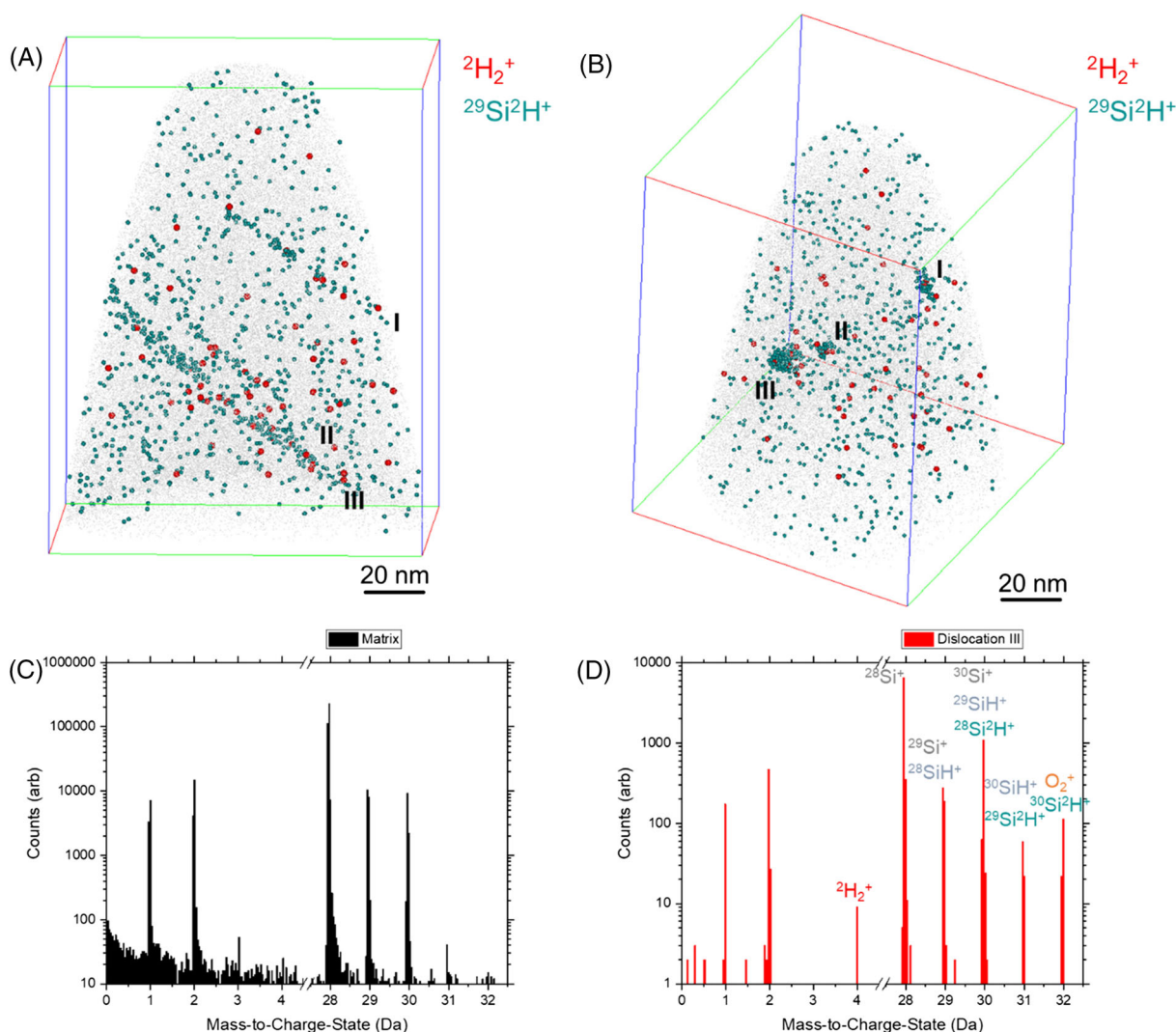


**FIGURE 2** Atom probe tomography (APT) datasets showing the enrichment of  $^2\text{H}_2^+$  and  $^{29}\text{Si}^2\text{H}^+$  at three individual dislocations, with a small fraction of Si atoms (grey) shown for reference. A, Viewing perpendicular to the dislocation. B, Viewing along the length of the dislocations. C, Mass spectra of the matrix of the APT specimen shown in (A). D, Mass spectra of dislocation III, showing clear enrichment in  $^2\text{H}$  at 4, 31, and 32 Da

the  $^2\text{H}$  signal. A relatively high ion detection rate was selected to increase the signal-to-noise ratio for the detection of low levels of impurities.<sup>33</sup>

### 3 | RESULTS

Figure 1 shows the analysis applied to a random-angle grain boundary isolated within the hydrogenated silicon. This type of grain boundary is known to be electrically active but also susceptible to hydrogen passivation.<sup>7</sup> Figure 1A presents an SEM image of the silicon wafer surface, with the etch pits formed during Secco etching marking the grain boundaries clearly visible. The grain boundary was then lifted out using FIB methods described in Lotharukpong et al.,<sup>29</sup> to produce the sharp needle-shaped geometry required for APT (Figure 1B).

Figure 1C shows a TKD image of the needle, used to ensure the alignment of the grain boundary along the axis of the needle and to characterise the misorientation and rotation axis of the boundary. In Figure 1D, an APT map showing hydrogen, unambiguously detected in the form of  $^2\text{H}_2^+$  ions at 4 Da in the APT mass spectrum, can be observed to segregate at the grain boundary. Additional hydrogen was also detected in the form of  $^{28}\text{Si}^2\text{H}^+$  at 30 Da,  $^{29}\text{Si}^2\text{H}^+$  at 31 Da, and  $^{30}\text{Si}^2\text{H}^+$  at 32 Da.

Within the same  $^2\text{H}$ -charged silicon sample, hydrogen was also found at three dislocations close to a twin boundary, as presented in Figure 2. These are observable both perpendicular (Figure 2A) and parallel (Figure 2B) to the dislocation line direction. A clear enrichment of  $^2\text{H}_2^+$  is observed at the dislocations, but a much greater quantity of hydrogen is detected in the form of  $\text{Si}^2\text{H}^+$  ions. The results in Figure 2 unambiguously demonstrate hydrogen segregating to dislocations in

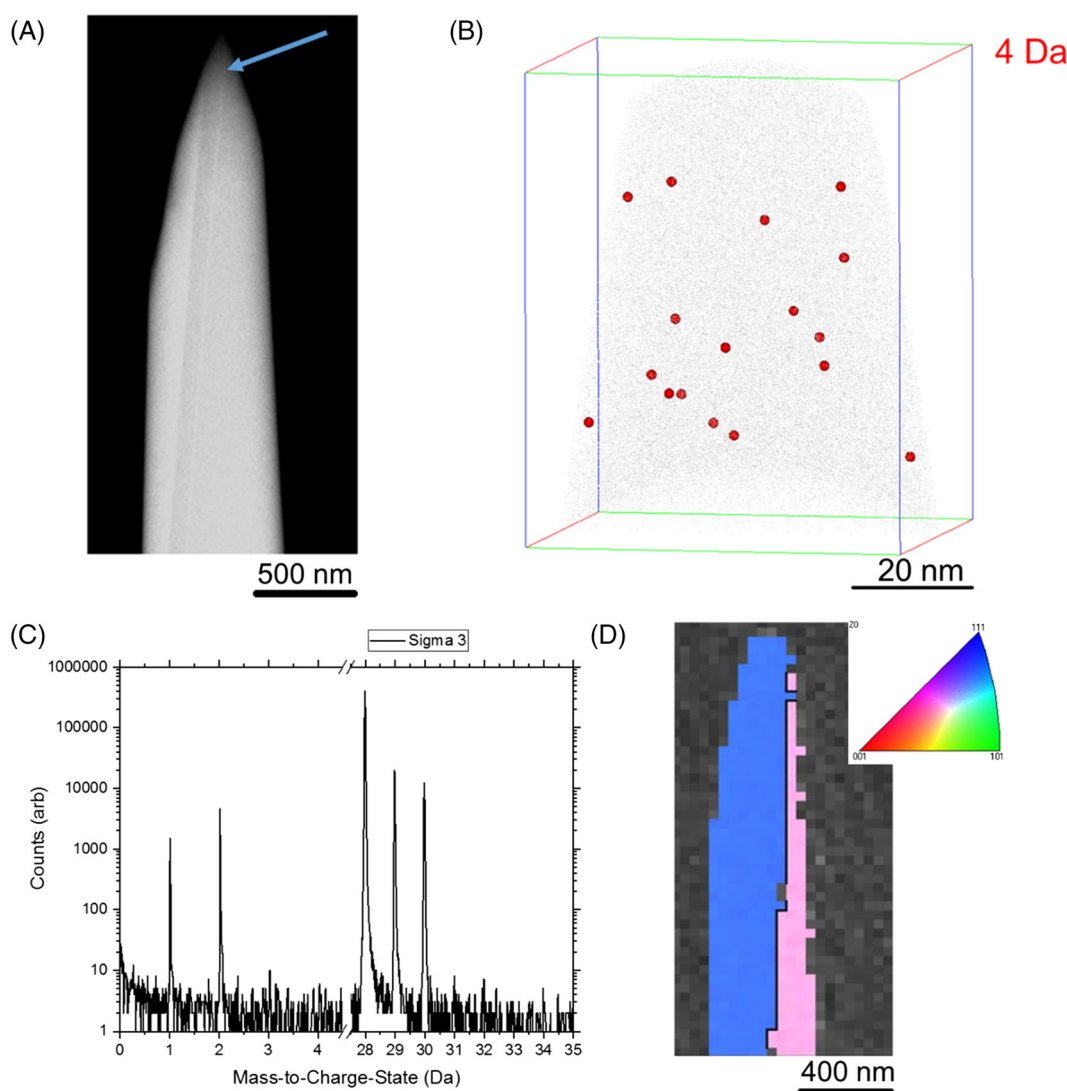


**FIGURE 3** A, Forward scatter image of a needle prior to atom probe tomography (APT) analysis, with the grain boundary marked. B, APT dataset of the needle analysed containing a  $\Sigma 3$  grain boundary, with the signal of  $^2\text{H}$  shown to be background noise (with a small fraction of Si in grey shown for reference). C, Mass spectra of the  $\Sigma 3$  grain boundary containing dataset. D, Transmission Kikuchi diffraction (TKD) of the needle prior to APT analysis. The needle was polished to ensure the grain boundary was at the apex of the needle

mc-Si and correlate well with the reduction in recombination activity of dislocations observed after hydrogen passivation.<sup>12,28</sup>

In contrast to dislocations, perfectly coherent  $\Sigma 3$  twin boundaries are known to be electrically inactive in mc-Si.<sup>34</sup> However, it is not known whether hydrogen segregates to these boundaries during passivation. Figure 3 displays a forward scattered image showing the dislocation free  $\Sigma 3$  twin boundary, extracted from a  $^2\text{H}$ -charged mc-Si wafer, and corresponding dataset. This boundary was characterised via TKD (Figure 3d), which was essential in confirming the presence of the grain boundary in the dataset and also the boundary type. No enrichment of  $^2\text{H}_2^+$  or indeed any other impurities, such as carbon, oxygen, or transition elements, are observed at this boundary.

## 4 | DISCUSSION AND ANALYSIS

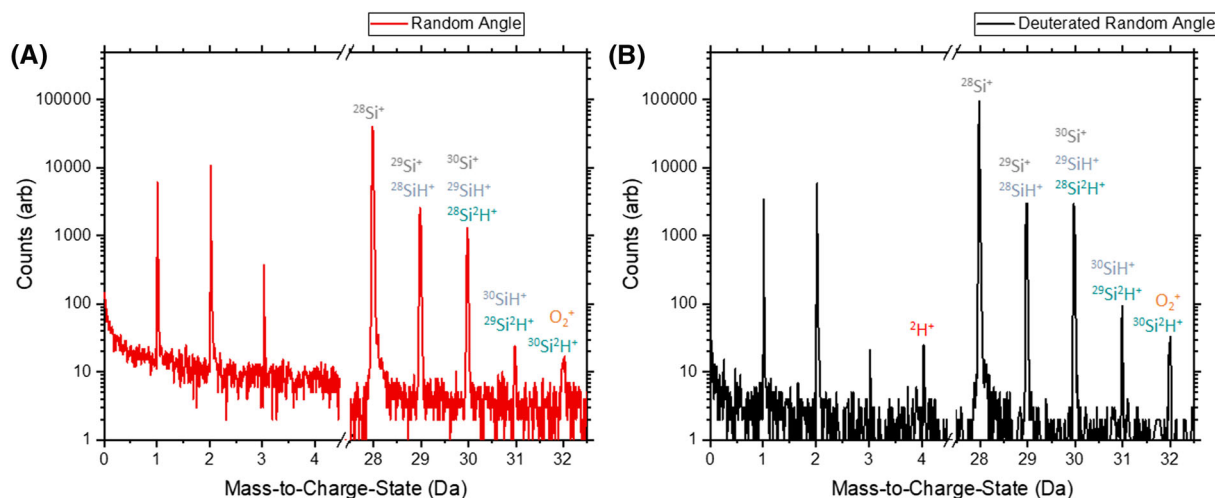
By extracting regions of interest and their corresponding mass spectra, it is possible to produce a quantitative estimation for the total amount of  $^2\text{H}$  present at individual grain boundaries and dislocations. This can then be used in future studies to determine if there is a correlation between the quantity of hydrogen at different crystallographic defects and electrical activities before and after hydrogen passivation.

Figure 4 presents the mass spectra for a deuterated and non-deuterated random-angle grain boundary. These datasets were acquired using the same experimental conditions. Using the  $[\text{Si}^+]$  to  $[\text{Si}^{2+}]$  ratios for both datasets, the electric field at the needle apex for both specimens can be approximated to  $19 \text{ Vnm}^{-1}$  (see Kingham<sup>35</sup>). In addition to the presence of the unambiguous  $^2\text{H}_2^+$  peak at 4 Da, it can be seen that the deuterated sample also exhibits significantly higher peaks at 30, 31, and 32 Da relative to the  $^{28}\text{Si}^+$  and  $^{29}\text{Si}^+$  peaks. While the peak at 4 Da is unambiguously due to  $^2\text{H}_2^+$  ions, this only represents a fraction of the total  $^2\text{H}$  detected in the APT experiment. The majority of  $^2\text{H}$  is detected as  $\text{Si}^{2+}\text{H}^+$  ions, contributing to the peaks at 30, 31, and 32 Da. However, these overlap with the

detection of other ions, eg,  $^{28}\text{Si}^{2+}\text{H}^+$  and  $^{30}\text{Si}^+$  at 30 Da; therefore, a deconvolution analysis must be applied to estimate the contribution of the  $^2\text{H}$  containing ions to each of these peaks.

By assuming that the isotopes of silicon are observed in their natural relative abundances,<sup>36</sup> and the fact that the  $^{28}\text{Si}^+$  peak has no significant overlaps in this system, it is possible to determine the relative contributions to these peaks. This deconvolution was performed by extracting a region of interest from the dataset containing an area of the grain boundary or along the length of a dislocation. Then using the programme AtomProbeLab (<https://sourceforge.net/projects/atomprobelab/>), which uses the maximum likelihood method, the quantity of  $^2\text{H}$  present was determined within confidence intervals (95% in this study), as described in London et al.<sup>37</sup> Since the detector has an efficiency of only 52%, a calculation of dividing the number of counts by 0.52 was required to determine the total number of  $^2\text{H}^+$  ions present. This deconvolution of the peaks maximised the likelihood of composition, based on the atomic abundance of silicon and the counts in the ranges (28–32 Da). From performing the deconvolution, it was determined that the vast majority of  $^2\text{H}$  was evaporated as  $\text{Si}^{2+}\text{H}^+$ , with less than 1% of  $^2\text{H}$  present in the 4-Da peak. Therefore, the values for  $^2\text{H}$  present at individual defects were given only with regard to  $^2\text{H}$  detected as  $\text{Si}^{2+}\text{H}^+$  and do not take into account  $^2\text{H}$  present at 2, 3, and 4 Da. Hence, the values given for  $^2\text{H}$  present should be viewed as lower estimates for the quantity present.

Table 1 shows the calculated Gibbsian interfacial excess quantities of  $^2\text{H}$  present, at the random-angle grain boundary and along each of the three dislocations as described in Miller and Smith.<sup>38</sup> Dislocation III is clearly shown to have the largest quantity of  $^2\text{H}$  along the length sampled, as might be expected from the dataset presented in Figure 2. Although this study does not allow for the determination of the cause of the variation between dislocations, it clearly shows the ability of the deconvolution method to allow for quantitative comparisons regarding the magnitude of the hydrogen present to be made. To give a rough estimation of number of  $^2\text{H}$  per atomic site along the dislocations,



**FIGURE 4** A, Mass spectra of a random-angle grain boundary from a sample, which has not received any hydrogen treatment. B, Mass spectra of the random-angle grain boundary shown in Figure 1, from a sample that has been passivated by  $^2\text{H}$

**TABLE 1** Quantity of  $^2\text{H}$  calculated as a Gibbsian interfacial excess for the random angle-grain boundary shown in Figure 1, for the three dislocations shown in Figure 2 and for the  $\Sigma 3$  grain boundary shown in Figure 3

	RA	$\Sigma 3$	I	II	III
$^2\text{H}$ quantified	$1.4 \pm 0.15 \times 10^{14}$ counts $\text{cm}^{-2}$	Below detection limit $\approx 2 \times 10^{12}$ counts $\text{cm}^{-2}$	$14 \pm 1.5$ counts $\text{nm}^{-1}$	$13 \pm 2$ counts $\text{nm}^{-1}$	$22 \pm 1.5$ counts $\text{nm}^{-1}$

Note. Upper and lower bounds are determined, within 95% confidence intervals. RA, random angle.

[Correction added on 19 August 2019, after first online publication: the columns in Table 1 were incorrectly aligned and this has now been corrected.]

the Burgers vector of a standard  $[110]$  dislocation was used. This dislocation type was chosen, representing an undissociated Lomer dislocation, since they are well known and extremely deleterious to silicon solar cells.<sup>39</sup> In this case, dislocations I and II have  $\approx 5$   $^2\text{H}$  ions per atomic site and dislocation III has  $\approx 8$   $^2\text{H}$  ions per atomic site. Since this is a rough estimation, with the types of dislocations not measured, these values can only be given as reference and must be studied further.

In this study, a high yield of APT specimens successfully analysed containing  $^2\text{H}$ -enriched grain boundaries was achieved. Although previous studies investigating the distribution of  $^2\text{H}$  in steels have utilised cryogenic transport to increase the quantity of  $^2\text{H}$  measured at crystallographic defects,<sup>24</sup> we believe this unnecessary since  $^2\text{H}$  has to be chemically bounded at the defect for passivation to occur. However, statistical certainty for the quantity of  $^2\text{H}$  present can be improved via the sampling of large lengths of grain boundaries, using the method discussed in Lotharukpong et al.<sup>29</sup>

## 5 | CONCLUSION

The ability to quantify the amount of hydrogen present at a grain boundary or dislocation is an important breakthrough for the characterisation of hydrogenation in mc-Si for solar cell applications. With regard to electrically active grain boundaries that are less susceptible to hydrogen passivation, it will allow determination of whether this is due to a lesser affinity of hydrogen to segregate at these features or if there are other causes such as the presence of specific impurities that are not passivated. The technique is also applicable to the crystallographic defects that limit the performance of cast monocrystalline solar cells.

This information is invaluable for informing the further development of casting methods for crystalline silicon growth in order to avoid the formation of defects that cannot be passivated.<sup>2,25</sup> It can also be observed how specific processing conditions, such as temperature and carrier injection,<sup>13,40</sup> can either increase or decrease the amount of hydrogen present at crystallographic defects. A better understanding of these effects is critical for optimising such processes and continuing to improve the performance of solar cells based on these materials.

## ACKNOWLEDGEMENT

This work has been supported by the UK Government through the EPSRC (Supersilicon grant, EP/M024911/1). The research materials supporting this paper can be accessed at ora.ox.ac.uk under the paper title.

## ORCID

David Tweddle  <https://orcid.org/0000-0001-6639-4477>

Phillip Hamer  <https://orcid.org/0000-0003-2168-4053>

## REFERENCES

1. "International technology roadmap for photovoltaic (ITRPV)—results 2017," vol. 9, no. March, 2018.
2. Castellanos S, Ekström KE, Autruffe A, et al. High-performance and traditional multicrystalline silicon: comparing gettering responses and lifetime-limiting defects. *IEEE J Photovoltaics*. 2016;6(3):1-19.
3. Adamczyk K, Sondena R, Stokkan G, et al. Recombination strength of dislocations in high-performance multicrystalline/quasi-mono hybrid wafers during solar cell processing. *Phys Status Solidi*. 2017;215(2):1-8.
4. Altermatt PP, Xiong Z, He QX, et al. High-performance p-type multicrystalline silicon (mc-Si): its characterization and projected performance in PERC solar cells. *Sol Energy*, no. In Press. 2018;175:68-74.
5. Sheoran M, Upadhyaya A, Rohatgi A. Bulk lifetime and efficiency enhancement due to gettering and hydrogenation of defects during cast multicrystalline silicon solar cell fabrication. *Solid State Electron*. 2008;52(5):612-617.
6. Martinuzzi S, Périchaud I, Warchol F. Hydrogen passivation of defects in multicrystalline silicon solar cells. *Sol Energy Mater Sol Cells*. 2003;80(3):343-353.
7. Chen J, Yang D, Xi Z, Sekiguchi T. Electron-beam-induced current study of hydrogen passivation on grain boundaries in multicrystalline silicon: influence of GB character and impurity contamination. *Phys B Condens Matter*. 2005;364(1-4):162-169.
8. Bertoni MI, Hudelson S, Newman BK, et al. Influence of defect type on hydrogen passivation efficacy in multicrystalline silicon solar cells. *Prog Photovoltaics Res Appl*. 2011;19(2):187-191.
9. Karzel P, Ackermann M, Gröner L, et al. Dependence of phosphorus gettering and hydrogen passivation efficacy on grain boundary type in multicrystalline silicon. *J Appl Phys*. 2013;114(24):244902.
10. Stokkan G, Marisa DS, Søndena R, et al. Impurity control in high performance multicrystalline silicon. *Phys Status Solidi Appl Mater Sci*. 2017;214(7):1700319.
11. Gindner S, Karzel P, Herzog B, Hahn G. Efficacy of phosphorus gettering and hydrogenation in multicrystalline silicon. *IEEE J Photovoltaics*. 2014;4(4):1063-1070.
12. Geerligs LJ, Komatsu Y, Röver I, Wambach K, Yamaga I, Saitoh T. Precipitates and hydrogen passivation at crystal defects in n- and p-type multicrystalline silicon. *J Appl Phys*. 2007;102(9):093702.
13. Hamer P, Hallam B, Wenham S, Abbott M. Manipulation of hydrogen charge states for passivation of P-type wafers in photovoltaics. *IEEE J Photovoltaics*. 2014;4(5):1252-1260.
14. Hahn G, Schönecker A, Burgers A, Ginige R, Cherkaoui K, Karg D. Hydrogen kinetics in crystalline silicon-PECVD SiN studies in mc and

- Cz silicon. *Proc 20th Eur Photovolt Sol Energy Conf Exhib.* 2005;1:717-720.
15. Stavola M, Kleekajai S, Wen L, et al. IR characterization of hydrogen in crystalline silicon solar cells. *Phys B Condens Matter.* 2009;404(23-24):5066-5070.
  16. Hahn G, Sontag D, Seren S, et al. Detection of hydrogen in multicrystalline silicon. *14th NREL Work Cryst Silicon Sol Cells Modul Mater Process.* 2004;1:129-133.
  17. Stoffers A, Barthel J, Liebscher CH, et al. Correlating atom probe tomography with atomic-resolved scanning transmission electron microscopy: example of segregation at silicon grain boundaries. *Microsc Microanal.* 2017;23:1-9.
  18. Stoffers A, Ziebarth B, Barthel J, Cojocar-Mirédin O, Elsässer C, Raabe D. Complex nanotwin substructure of an asymmetric  $\Sigma 9$  tilt grain boundary in a silicon polycrystal. *Phys Rev Lett.* 2015;115(23):1-5.
  19. Stoffers A, Cojocar-Mirédin O, Breitenstein O, Seifert W, Zaefferer S, Raabe D. "Grain boundary characterization in multicrystalline silicon using joint EBSD, EBIC, and atom probe tomography," *2014 IEEE 40th Photovolt. Spec. Conf.*, pp. 0042-0046, 2014.
  20. Stoffers A, Cojocar-Mirédin O, Seifert W, Zaefferer S, Riepe S, Raabe D. Grain boundary segregation in multicrystalline silicon: correlative characterization by EBSD, EBIC, and atom probe tomography. *Prog Photovoltaics Res Appl.* Dec. 2015;23(12):1742-1753.
  21. Ohno Y, Kutsukake K, Deura M, et al. Recombination activity of nickel, copper, and oxygen atoms segregating at grain boundaries in mono-like silicon crystals. *Appl Phys Lett.* 2016;109(14):142105.
  22. Sundell G, Thuvander M, Yatim AK, Nordin H, Andrén HO. Direct observation of hydrogen and deuterium in oxide grain boundaries in corroded Zirconium alloys. *Corros Sci.* 2015;90:1-4.
  23. Takahashi J, Kawakami K, Kobayashi Y, Tarui T. The first direct observation of hydrogen trapping sites in TiC precipitation-hardening steel through atom probe tomography. *Scr Mater.* 2010;63(3):261-264.
  24. Chen YS, Haley D, Gerstl SSA, et al. Direct observation of individual hydrogen atoms at trapping sites in a ferritic steel. *Science (80-).* 2017;355(6330):1196-1199.
  25. Stokkan G, Hu Y, Mjøs O, Juel M. Study of evolution of dislocation clusters in high performance multicrystalline silicon. *Sol Energy Mater Sol Cells.* 2014;130:679-685.
  26. Secco d' Aragona F. Dislocation etch for (100) planes in silicon. *J Electrochem Soc.* 1972;119(7):948.
  27. Johnson NM, Biegelsen DK, Moyer MD. Deuterium passivation of grain-boundary dangling bonds in silicon thin films. *Appl Phys Lett.* 1982;40(10):882-884.
  28. Duerinckx F, Szlufcik J. Defect passivation of industrial multicrystalline solar cells based on PECVD silicon nitride. *Sol Energy Mater Sol Cells.* 2002;72(1-4):231-246.
  29. Lotharukpong C, Tweddle D, Martin TL, et al. Specimen preparation methods for elemental characterisation of grain boundaries and isolated dislocations in multicrystalline silicon using atom probe tomography. *Mater Charact.* 2017;131:472-479.
  30. Rice KP, Chen Y, Prosa TJ, Larson DJ. Implementing transmission electron backscatter diffraction for atom probe tomography. *Microsc Microanal.* 2016;22(3):583-588.
  31. Babinsky K, Knabl W, Lorch A, De Kloe R, Clemens H, Primig S. Grain boundary study of technically pure molybdenum by combining APT and TKD. *Ultramicroscopy.* 2015;159:445-451.
  32. Barba D, Pedrazzini S, Vilalta-Clemente A, et al. On the composition of microtwins in a single crystal Ni-based superalloy. *Scr Mater.* 2017;127:37-40.
  33. Seol J, Kim Y, Park C. A brief comment on atom probe tomography applications. *Appl Microsc.* 2016;46(3):127-133.
  34. Chen B, Chen J, Sekiguchi T, Saito M, Kimoto K. Structural characterization and iron detection at  $\Sigma 3$  grain boundaries in multicrystalline silicon. *J Appl Phys.* 2009;105(11):1-6.
  35. Kingham DR. The post-ionization of field evaporated ions: a theoretical explanation of multiple charge states. *Surf Sci.* 1982;116(2):273-301.
  36. Bièvre P, Gallet M, Holden NE, Barnes IL. Isotopic abundances and atomic weights of the elements. *J Phys Chem Ref Data Monogr.* 1984;13(3):809-891.
  37. London AJ, Haley D, Moody MP. Single-ion deconvolution of mass peak overlaps for atom probe microscopy. *Microsc Microanal.* 2017;23(2):300-306.
  38. Miller MK, Smith GDW. Atom probe analysis of interfacial segregation. *Appl Surf Sci.* 1995;87-88(94):243-250.
  39. Bauer J, Hahnel A, Werner P, et al. Recombination at Lomer dislocations in multicrystalline silicon for solar cells. *IEEE J Photovoltaics.* 2016;6(1):100-110.
  40. Lee SH, Bhopal MF, Lee DW, Lee SH. Review of advanced hydrogen passivation for high efficient crystalline silicon solar cells. *Mater Sci Semicond Process.* 2018;79(January):66-73.

**How to cite this article:** Tweddle D, Hamer P, Shen Z, Markevich VP, Moody MP, Wilshaw PR. Direct observation of hydrogen at defects in multicrystalline silicon. *Prog Photovolt Res Appl.* 2021;29(11):1158-1164. <https://doi.org/10.1002/pip.3184>